Journal of the Meteorological Society of Japan, Vol. 94, No. 1, pp. 7−24, 2016
DOI:10.2151/jmsj.2016-001

Predictability Changes of Stratospheric Circulations in Northern Hemisphere Winter

Tomoko ICHIMARU

Research Department, Remote Sensing Technology Center of Japan, Tsukuba, Japan

Shunsuke NOGUCHI

Graduate School of Science, Kyoto University, Kyoto, Japan

Toshihiko HIROOKA

Department of Earth and Planetary Sciences, Kyushu University, Fukuoka, Japan

and

Hitoshi MUKOUGAWA

Disaster Prevention Research Institute, Kyoto University, Uji, Japan

(Manuscript received 13 June 2015, in final form 16 September 2015)

Abstract

Practical predictability of the stratospheric circulation in the boreal winters during the period 2001–2006 has been examined using the archive of 1-month ensemble forecast datasets provided by the Japan Meteorological Agency. To investigate the predictability limit, two measures of the Root-Mean-Square Error (RMSE) and Anomaly Correlation (AC) have been used for the 10-hPa geopotential height field. In the winter stratosphere, an intermittent character of planetary wave activity causes two specific periods of the stratospheric circulation, i.e., an undisturbed phase with inactive planetary waves and a disturbed phase with active ones. Therefore, the predictability needs to be evaluated taking account of this feature. On the basis of careful consideration, the mean predictable period can be estimated to about 10 days during the disturbed phase; it is longer than the tropospheric predictable period of about 7 days. However, it exhibits large variability because of different growth rates of forecast errors caused by contributions of both wave and zonal-mean fields. During the undisturbed phase, the predictable period based on the AC is almost the same as that of the disturbed phase, although the predictable period based on the RMSE is extremely long, since the RMSE predictability is measured against the climatological standard deviation affected by disturbed phases. Therefore, the horizontal pattern of the stratospheric circulation is less predictable even though the forecast error is quite small.

Keywords predictability; stratospheric sudden warming; stratospheric circulation

Corresponding author: Toshihiko Hirooka, Department of Earth and Planetary Sciences, Kyushu University, 744 Motooka, Nishi-ku, Fukuoka 819-0395, Japan
E-mail: hirook@geo.kyushu-u.ac.jp

1. Introduction

Future atmospheric conditions cannot be perfectly predicted even on the basis of a state-of-the-art numerical weather prediction model. To examine the predictability of such atmospheric conditions is a challenging subject, since Lorenz (1963) revealed the chaotic character of the atmosphere.

Forecast skill of weather prediction models depends not only on the accuracy of initial conditions and the realism of the model, but also on nature of nonlinear atmospheric flows themselves. The initial errors, even if they were infinitesimal, steadily amplify and lead to a total loss of skill in the weather forecast after a finite forecast period. The forecast by a perfect model has an inevitable predictable limit because of the growth of initial errors due to intrinsic unstable characteristics of atmospheric motions. Thus, the predictability has been an important issue for the numerical forecast, even if the forecast skill has gradually progressed. In particular, the predictability of large-scale atmospheric motions is one of main themes concerning nonlinear dynamics of the atmosphere and many studies have been devoted to this subject (e.g., Lorenz 1963; Kimoto et al. 1992; Kalnay 2003, for a review). In the troposphere, the forecast skill has been improved owing to the social demand, and now the practical predictability limit is estimated to about 7 days (Kalnay 2003).

An important impact of the stratosphere on the tropospheric circulation was first acknowledged by pioneering works of Boville (1984) and Kodera et al. (1990). Then, Baldwin and Dunkerton (2001) pointed out characteristics of the downward migration for the annular mode variation from the stratosphere to the troposphere, which enhanced our expectation to improve the forecast skill of the extended-range prediction in the troposphere by adequately incorporating the stratospheric circulation anomaly. In fact, such skill improvement during a stratospheric sudden warming (SSW) event was demonstrated by Reichler et al. (2005) and Kuroda (2008). In addition, the predictability of the stratosphere during the occurrence periods of SSW events quickly has attracted much interest (e.g., Mukougawa and Hirooka 2004; Mukougawa et al. 2005; Marshall and Scaife 2010), as described below.

Recently, a comprehensive review on a powerful impact on the weather exerted by the stratosphere was made by Kidston et al. (2015). Tripathi et al. (2015) also reviewed several studies on the predictability of stratospheric extreme vortex events and their possible effects on the tropospheric forecast skill.

The SSW event, discovered by Scherhag in 1952 (Scherhag 1952), is a spectacular phenomenon in which westerlies associated with the polar vortex in the boreal winter abruptly slow down or even reverse their direction, accompanied by a rise of stratospheric polar temperatures by several tens of kelvins. Since this discovery, SSW events have been spiritedly monitored, and many studies have investigated them to clarify the mechanism, stemming from the pioneering paper by Matsuno (1971), using global stratospheric data obtained by instruments on board satellites since the early 1970s. In the 1980s, SSW events came to be successfully simulated by numerical models, including the stratosphere (e.g., Mechoso et al. 1985). Eventually in the 1990s, operational stratospheric assimilation system started in UK Met Office (Swinbank and O'Neill 1994). Since then stratospheric circulations including SSW events have been predicted by various operational models, which have been improved year after year.

Mukougawa and Hirooka (2004) (hereafter, MH04) first examined the predictability on the basis of a state-of-the-art numerical weather prediction model. They estimated the predictability limit of the stratospheric circulation in the 1998/99 winter, during which an SSW occurred in December 1998, by the use of 1-month extended-range forecasts issued once a week by the Japan Meteorological Agency (JMA). The Root Mean Square Error (RMSE) evolution of the 10-hPa geopotential height was found to show the predictable period longer than 20 days. It was also revealed that the RMSE was enlarged during the SSW and then the circulation was difficult to predict, which was mainly caused by the poor prediction of the phase of planetary waves, i.e., the location of their troughs and ridges.

Mukougawa et al. (2005) further investigated the predictability of a major warming in December 2001 using all ensemble members of the JMA 1-month forecasts. They reported that the warming peak was predictable at least from 2 weeks in advance in terms of the 10-hPa zonal-mean temperature at 80°N. However, Hirooka et al. (2007) dealt with a SSW event in January 2004 and showed a rather limited predictable period of 9 days. They also suggested that the predictability would depend on the occurrence pattern of SSW events. Thus, these previous studies show that the predictable period of the stratospheric circulation ranges from 9 to 20 days, which may be significantly longer than that of the tropospheric circulation of about 7 days. However, analyses are

limited to a few cases, and our knowledge on the predictability of the stratospheric motions is still fragmentary.

Stan and Straus (2009) discussed the predictability in the stratosphere and troposphere on the basis of normalized forecast errors due to both phase and amplitude differences between forecasted and observed waves using the National Centers for Environmental Prediction (NCEP) Climate Forecast System Interactive Ensemble. They reported that one of the main factors limiting the predictability was errors in the wave phase. However, the forecast errors associated with zonal-mean fields were not discussed in their paper, even though the zonal-mean field also greatly varies during occurrence periods of SSW events.

In the present study, more extensive analyses are performed using the archive of ensemble 1-month forecast data obtained by a JMA operational prediction system (Japan Meteorological Agency 2002). The purpose of the present study is to statistically reveal the predictability of stratospheric circulations. However, the nature of large day-to-day variability in the stratospheric circulation would make it difficult to apply the method in the troposphere directly to the stratosphere for estimates of the predictability. Thus, we propose how to estimate the stratospheric predictability, taking into account of this nature. The predictability is estimated on the basis of the RMSE, which is considered as a measure of "distance" between the predicted and the observed geopotential heights in phase space, as well as the Anomaly Correlation (AC) which shows a "pattern correlation" between forecasted and observed anomalies of geopotential height.

2. Data and model

The operational ensemble 1-month (34-day) forecast datasets provided by JMA are used for boreal winters (December-February) from 2001/02 to 2005/06 since the model was considerably changed in March 2001 and March 2006. During this period, the JMA ensemble 1-month prediction was carried out at 1200 UTC every Wednesday and Thursday from 12 perturbed and 1 unperturbed initial conditions. Numerical integrations were conducted using a JMA global spectral model with a triangular truncation at total wavenumber 106 (T106) and 40 hybrid sigma-pressure vertical levels up to 0.4 hPa. Physical processes important for the stratosphere, such as radiation (Briegleb 1992), gravity wave drag (Iwasaki et al. 1989), and a direct aerosol effect for radiation (Coakley et al. 1983) are also implemented. For further model details, the reader should refer to Japan Meteorological Agency (2002).

The initial perturbations are obtained using the Breeding of Growing Modes (BGM) method (Toth and Kalnay 1993). They are applied at all pressure levels north of 20°N with an amplitude set to be 14.5 % of the climatological root-mean-square variance at 500 hPa height. An ensemble mean denotes an average of all 13 ensemble members on each day. The data were archived daily at 1200 UTC for the 34-day prediction period on a 2.5 × 2.5 longitude-latitude grid at 22 levels from 1000 to 1 hPa.

To verify this model, we use a JMA Global Analysis dataset with 1.25-degree horizontal resolution at 1200 UTC on 23 levels from 1000 to 0.4 hPa. In the computation, its horizontal resolution is fitted to that of the forecast data.

3. Analysis methods

3.1 RMSE analysis

The RMSE at lead time t is defined as the following equation:

$$\sigma(t) = \left[\frac{\sum_{i=1}^{N} (z_{fi}(t) - z_{ai}(t))^2 \cos\phi_i}{\sum_{i=1}^{N} \cos\phi_i} \right]^{\frac{1}{2}}, \tag{1}$$

where ϕ_i is latitude of i-th grid and $\cos\phi_i$ means latitudinal weighting. z_{fi} and z_{ai} indicate the ensemble-mean forecast and the analysis of the geopotential height on i-th grid point, respectively. N is the number of grid points and $\sigma(t)$ is averaged over latitudes north of 20°N. The RMSE indicates a distance between the forecast and the observation in phase space.

The predictability limit based on the RMSE of the ensemble mean forecast is defined as the time when the RMSE surpasses a specified criterion which is defined from the magnitude of natural variability in the considered field. Note that the RMSE of the ensemble mean forecast approaches asymptotically to the climatological standard deviation (CSD). Here, the CSD is defined as the following equation:

$$\sigma_c = \left[\frac{\sum_{i=1}^{D}\sum_{i=1}^{N} (z_{ai}(t) - z_{ci})^2 \cos\phi_i}{D\sum_{i=1}^{N} \cos\phi_i} \right]^{\frac{1}{2}}, \tag{2}$$

where z_{ci} represents the climatological mean value

on the i-th grid point, and D is long duration defining climatology. In Section 5.1, we will carefully examine the criterion appropriate to the ensemble mean forecast in the stratosphere.

3.2 AC analysis

The AC at lead time t is defined as the following equation:

$$r(t) = \frac{\sum_{i=1}^{N}(z_{fi}(t)-z_{ci})(z_{ai}(t)-z_{ci})\cos\phi_i}{\sqrt{\sum_{i=1}^{N}(z_{fi}(t)-z_{ci})^2\cos\phi_i \sum_{i=1}^{N}(z_{ai}(t)-z_{ci})^2\cos\phi_i}}, \quad (3)$$

where z_{fi} and z_{ai} indicate the ensemble-mean forecast, respectively, and the observation of the geopotential height, and z_{ci} represents the observed climatological mean value on the i-th grid point. N is the number of grid points and $r(t)$ is averaged over latitudes north of 20°N. The AC indicates a measure of the similarity of synoptic patterns. The predictability limit based on the AC is defined as the time when the AC first attains 0.6 (e.g., Hollingsworth et al. 1978; Kalnay 2003).

3.3 Contribution ratio to the forecast error

In order to examine each contribution of the zonal-mean field, the wave amplitude, and the wave phase component to the forecast error, the mean square error (E_T) averaged over latitudes north of 20°N is divided into the mean square error associated with the zonal-mean field (E_Z), the wave amplitude (E_A), and the wave phase (E_P) using a Fourier decomposition according to Appendix of Stan and Straus (2009). Then, each contribution ratio of the zonal-mean field, the wave amplitude, and the wave phase to the forecast error is evaluated by E_Z/E_T, E_A/E_T, and E_P/E_T, respectively.

4. Features of stratospheric circulations

First, we analyze the seasonal marches at 10 hPa during boreal winters from 2001/02 to 2005/06. Figures 1a and 1b show time-latitude sections of the zonal-mean zonal wind ($\bar{U}$) and the zonal-mean temperature ($\bar{T}$) at 10 hPa, respectively. The shading denotes regions of easterlies in Fig. 1a and values exceeding 230 K in Fig. 1b. From these panels, we can see large interannual variations in the analysis period. Fig. 1a indicates that intermittent reversals of $\bar{U}$ frequently occur in higher latitudes except for the 2004/05 winter when the polar vortex was very strong in the stratosphere. On the other hand, interannual changes in lower latitudes are characterized by the appearance of westerly and easterly regimes in association with the quasi-biennial oscillation (QBO). The evolution of $\bar{T}$ in Fig. 1b is related to that of $\bar{U}$ through the thermal wind balance; warmings are observed in higher latitudes, corresponding to the zonal wind reversals.

Such variations of $\bar{U}$ and $\bar{T}$ reflect the occurrence of SSW events. A SSW event is generally defined on the basis of the World Meteorological Organization (WMO) definition. However, in order to extract independent SSW events, we apply a somewhat different definition from it in this study; SSW events are to be those that fulfill the following conditions on the basis of 10-hPa zonal-mean fields: The first condition is that warming peaks are separated by at least 10 days in order to extract independent SSWs. The second condition is that $\bar{T}$ averaged over latitudes north of 80°N rises more than 15 K in 3 days. The third condition is that $\bar{U}$ at 60°N reverses to easterlies. When an event certainly fulfills the first condition and at least satisfies the second or third conditions, it is defined here as an SSW event. Resultantly, we have ten SSW events in the analysis period from 2001/02 to 2005/06 boreal winters, as shown later in the second column of Table 1 with event numbers in the first column. In the other winters than the 2004/05 winter, a couple of SSW events were observed, while in the 2004/05 winter no evident warmings were seen until late February 2005.

Note that the number of defined SSW events during a period from 2001/02 to 2005/06 winter is ten, which is 2.5 times larger than that of major SSW events based on the definition of Charlton and Polvani (2007) as shown in Fig. 10a of Inatsu et al. (2015). This is because our definition of SSW events is lenient in comparison with that of major SSW events used in those studies.

From Figs. 1c and 1d showing time-latitude sections of the 10 hPa amplitude of zonal wavenumber (WN) 1 and 2 components, we can see intermittent intensification of planetary waves which causes SSW events. Thus, SSW events are classified in terms of the prominent zonal wavenumber component of planetary wave in the 10-hPa geopotential height field. Fourier decomposition is performed to obtain zonal harmonics. When a WN-1 component is prominent during the occurrence of an SSW, it is defined as a "WN-1 type". On the other hand, when a WN-2 component is prominent, it is defined as a "WN-2 type". In the case of the WN-2 type, the polar vortex is greatly elongated or

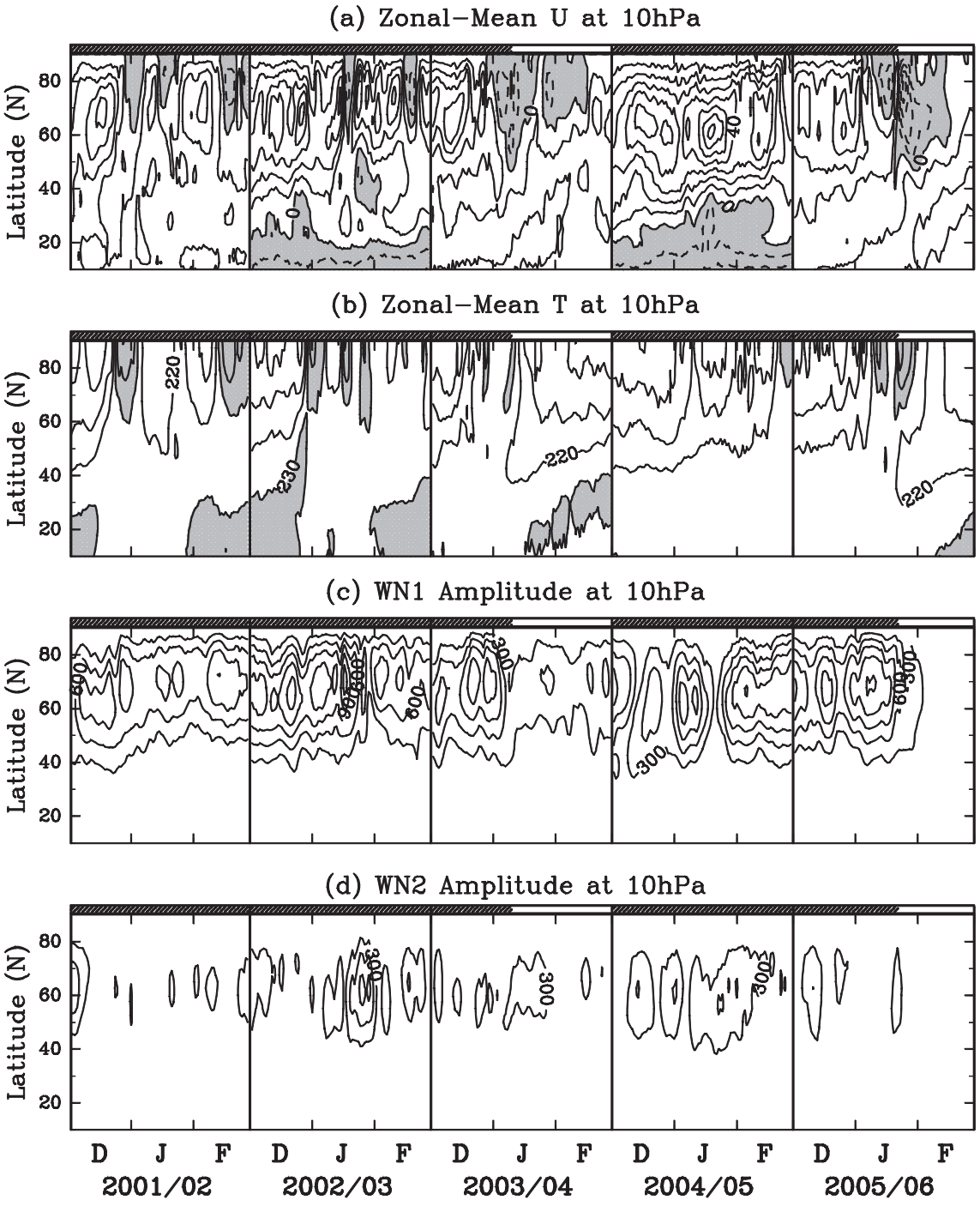

Fig. 1. Time-latitude cross sections of (a) $\bar{U}$, (b) $\bar{T}$, (c) WN-1 and (d) WN-2 amplitudes at 10 hPa in boreal winters from 2001/02 to 2005/06. The shading denotes regions of easterlies in (a) and values exceeding 230 K in (b). Contour intervals are (a) 10 m s^{-1}, (b) 10 K, (c) and (d) 300 m, respectively. The band above each panel shows two phases: disturbed (shaded) and undisturbed (unshaded) phases.

Table 1. SSW events occurring in boreal winters from 2001/02 to 2005/06 with "Event No." "Warming Peak" denotes the day when the 10-hPa averaged over the area north of 80°N attains a warming maximum. "Lead Time" shows the time length from the initial time of the forecast to each warming peak. Each predictability limit is evaluated on the basis of the RMSE for the forecast initialized about two weeks before the warming peak. See the text in Section 5.2 for details on the latter two time lengths.

Event No.	Warming Peak	Lead Time (days)	RMSE Limit (days)
1	27 Dec 2001	15	16
2	16 Feb 2002	17	15
3	1 Jan 2003	13	7
4	16 Jan 2003	15	10
5	26 Jan 2003	11	5
6	27 Dec 2003	16	12
7	10 Jan 2004	16	10
8	24 Feb 2005	15	8
9	12 Jan 2006	15	19
10	22 Jan 2006	17	11

separated into two centers.

As well known, the WN-1 component is predominant almost throughout winter season; it is found that most SSW events in the analysis period are essentially caused by intensification of WN-1 planetary waves, though WN-2 and WN-3 planetary waves (not shown) sometimes play an important role in some SSW events (Hirooka et al. 2007). The SSW in late January 2003 (No. 5 in Table 1) was not a typical vortex splitting event, but it can be classified into a WN-2 type SSW because of predominance of the WN 2 over the WN 1.

Furthermore, it is noted that both WN-1 and WN-2 amplitudes were very small after SSW events in January 2004 and January 2006 (Nos. 7 and 10 in Table 1). In these cases, the polar vortex was broken down and $\bar{U}$ changed to easterlies in the stratosphere. Thus, the vertical propagation of planetary waves from the troposphere would be prohibited. As a result, wave amplitudes in the stratosphere might become quite small.

These observations indicate that the time evolution of the stratospheric circulation can be roughly described by transitions between "disturbed" and "undisturbed" phases. The disturbed (undisturbed) phase could be characterized by enhanced (reduced) stratospheric planetary wave activity. The predominant process controlling the evolution of the stratospheric circulation would be also different between these two phases: Wave-mean flow interaction (radiative process) with a relatively short (long) characteristic time-scale would be the main contributor for the disturbed (undisturbed) phase. Hence, it is reasonably expected that characteristic of forecast error growth in the stratosphere is also largely different between these two phases. Based on this, here, we will discuss the forecast error evolution for each phase separately.

The disturbed (undisturbed) phase is defined when a "total amplitude" from WN 1 to 3 at 60°N and 10 hPa is larger (smaller) than 500 m. Here, the total amplitude A_0 is defined as

$$A_0 = \sqrt{\sum_{k=1}^{3}(a_k^2 + b_k^2)}, \tag{4}$$

where a_k and b_k are the cosine and sine coefficients of the zonal wavenumber k. Upper bands above each panel in Fig. 1 show disturbed phases (shaded) and undisturbed ones (unshaded). During the undisturbed phases, easterlies appear in higher latitudes for a while and after that the gradually decreases, returning to the cold polar region.

The disturbed phase is usually associated with weak westerlies, and SSW events occurred usually during this phase (cf. Fig. 5 and Table 1). It should also be remarked that the winter of 2004/05 is classified as the disturbed phase although the westerly prevails during this winter season as shown in Fig. 1a. Hence, stratospheric circulations during the disturbed phase with enhanced planetary waves are not necessarily characterized by weak westerlies.

5. Predictability

5.1 Predictability limit based on RMSE and AC

In this section, general characteristics of time

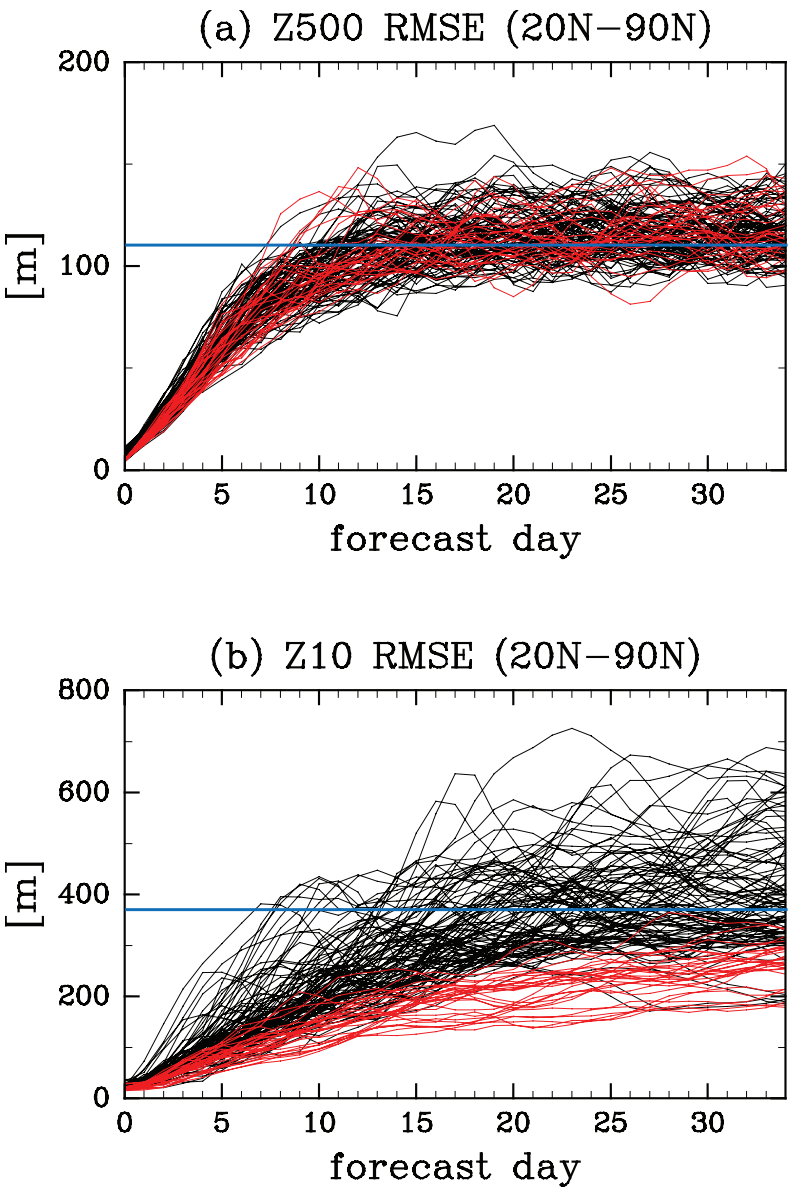

Fig. 2. Time evolutions of the RMSE in the geopotential height field [m] at (a) 500 hPa and (b) 10 hPa for 126 ensemble-mean forecasts performed for the five winters. Black and red lines denote the time evolution of the RMSE in the disturbed and the undisturbed stratospheric phases, respectively. Horizontal blue lines show the climatological standard deviation during the analysis period, for comparison. The value is 111 m in (a) and 368 m in (b). As for the climatological standard deviation, see the text.

evolution of the RMSE both in the troposphere and the stratosphere are firstly examined and a method to define the stratospheric criterion for predictability limit is discussed. Figure 2 shows time evolutions of the RMSE in the geopotential height field at (a) 500 hPa and (b) 10 hPa for 126 ensemble mean forecasts performed for the five winter seasons. Black and red lines indicate the RMSE in the disturbed and undisturbed phases classified in the stratosphere, respectively. Note that the score of zero means perfect skill of the prediction and the RMSE generally increases with forecast time.

From these panels, it is revealed that the tropospheric evolution of the RMSE little depends on the

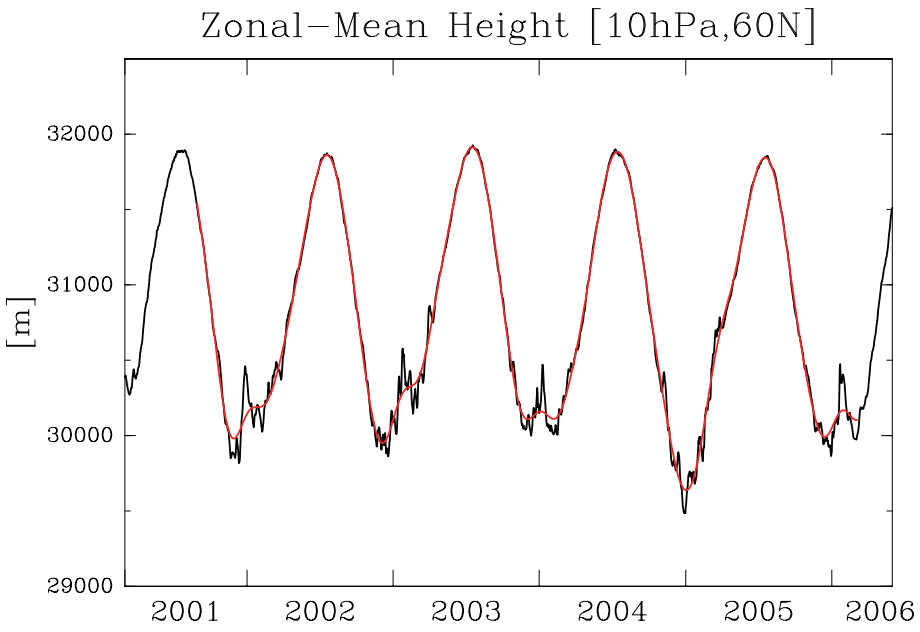

Fig. 3. Time variation of zonal-mean geopotential height [m] at 60°N and 10 hPa for the period from 1 Mar. 2001 to 30 Apr. 2006. Black and red lines represent the geopotential height and the low-pass filtered geopotential height, respectively. The used low-pass filter has a cutoff period of 90 days, which corresponds to the length of each winter period.

stratospheric phases (Fig. 2a), while the stratospheric one is clearly suppressed in the undisturbed phases compared with that in the disturbed phase (Fig. 2b). Therefore, the variance of the RMSE in the stratosphere is relatively larger than that in the troposphere. Moreover, it is found that the growth rate of the RMSE in the stratosphere is much slower than that in the troposphere.

As described in Section 3.1, the predictability limit based on the RMSE is estimated generally by the use of a specified threshold value which represents the magnitude of natural variability of the considered field. MH04, who first examined the stratospheric predictability for the 1998/99 winter based on the RMSE, calculated the climatological standard deviation (CSD) by the same method as that for the troposphere: They obtained the CSD by using the winter averaged field as the reference value z_{ci} in Eq. (2). However, since the stratospheric circulation has a huge interannual variability as well as its predominant seasonal march as described in the following, we have to define more carefully the CSD for the stratospheric circulation.

Figure 3 illustrates the time change of the zonal-mean geopotential height (black) and low-pass filtered geopotential height (red) at 60°N and 10 hPa for the period from 1 March 2001 to 30 April 2006. The low-pass filtered values are obtained by applying a numerical filter of which cutoff period is 90 days, corresponding to the length of each winter period. Hence, the observed height field is composed of long-term and short-term fluctuations which can be defined as anomalies from the low-pass filtered field.

It is known that variability of stratospheric circulations includes not only daily and intraseasonal variations but also very large interannual ones, i.e., variability due to the quasi-biennial oscillation, the 11-year sunspot cycle, the ENSO, and so on (Labitzke and van Loon 1999). This is also confirmed in our analysis period: The 10-hPa zonal-mean height in the 2004/05 winter was much lower than that in the other winters (Fig. 3). Under this circumstance, when the CSD is calculated using the 5-winter mean field as a reference field in Eq. (2), we encounter a serious problem as discussed below.

Figure 4 shows time evolutions of daily variance of 10-hPa anomalous heights on the basis of various reference fields in Eq. (2) averaged over the region north of 20°N. The reference fields are (a) the 5-winter mean, (b) the winter mean for each year, and (c) the low-pass filtered geopotential height field. From Fig. 4a, we can see that the magnitude of vari-

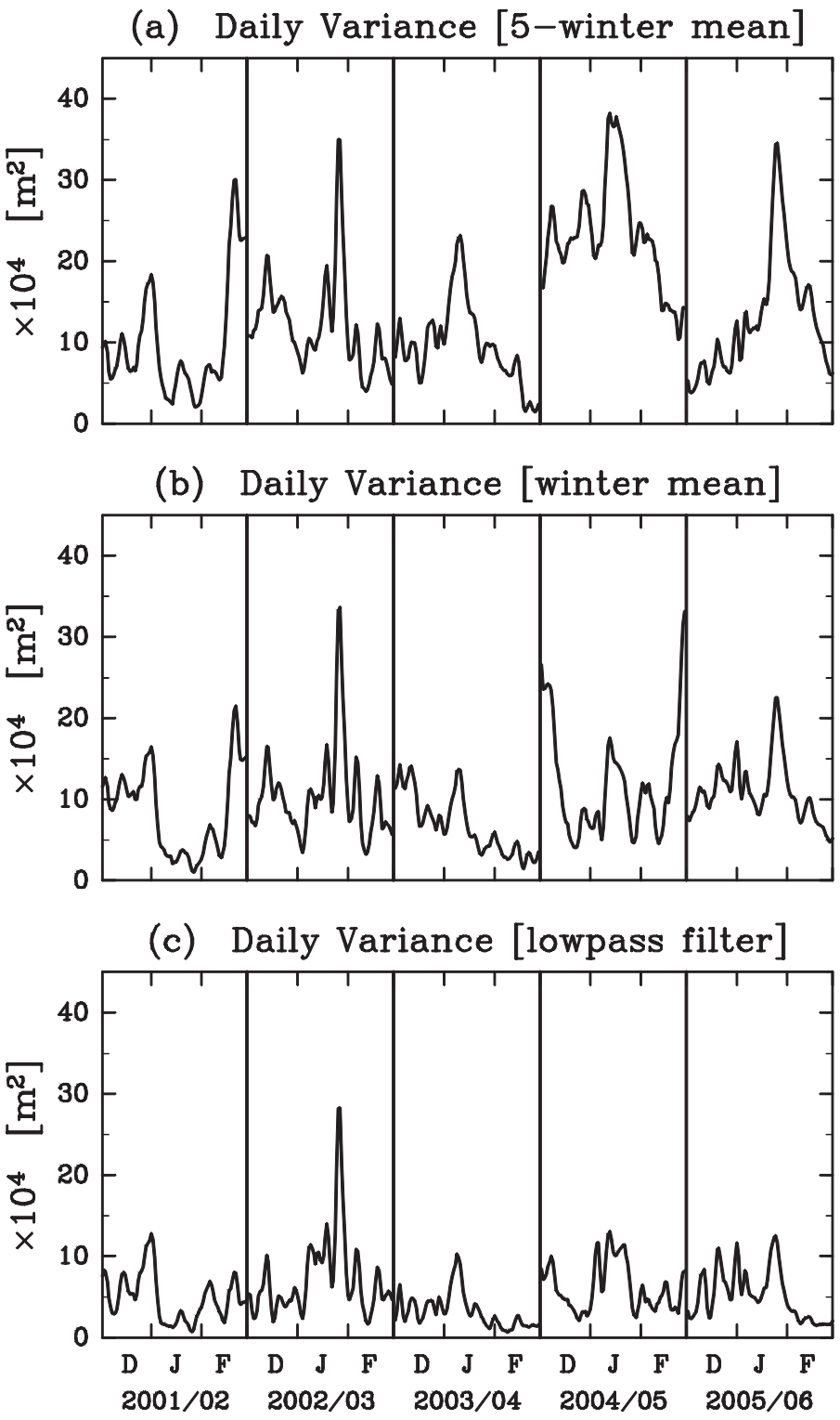

Fig. 4. Time evolution of daily variance [$\times 10^4$ m^2] of 10-hPa anomalous height field averaged over the region north of 20°N on the basis of various reference fields. The reference fields are (a) the 5-winter mean, (b) the winter mean for each year, and (c) the low-pass filtered field, respectively.

ance also varies interannually, reflecting large interannual variations of the winter mean field. In particular, it is found that the variance in the 2004/05 was much larger than that in other winters, because polar temperatures were colder and the polar vortex was stronger. The resultant CSD based on such large variance is 368 m (see Fig. 2b), which contains an influence of interannually fluctuated components. From Fig. 4b, in which the winter mean field for each year is used as the reference field, year-to-year change of variance is smaller than that in Fig. 4a. In this case, the CSD is estimated at 313 m; the value is almost the same as that calculated by MH04. However, the variance still includes the influence of intraseasonal fluctuations.

In the present study, ensemble 1-month (34-day) forecast datasets are used to estimate predictability limit associated with atmospheric motions shorter than the intraseasonal time scale. Therefore, we should use an appropriate reference field that well represents the natural variability shorter than the intraseasonal time scale. From Fig. 4c, in which the 90-day low-pass filtered field is used as the reference field, it is found that interannual and month-to-month change of variance is much smaller than that in Figs. 4a and 4b. The resultant value of the modified CSD is 232 m, and the value could represent the magnitude of natural variability shorter than the intraseasonal time scale. It is noted that daily variance in late January 2003 was about three times larger than that in the other periods. The large value is due to the dominant WN-2 amplitude (see Fig. 1d), whereas the low-pass filtered field features the predominance of WN 1 (not shown).

Now, the predictability limit based on the RMSE can be estimated for all the available forecasts by using the obtained threshold (232 m). Figure 5a illustrates the time evolution of observed $\bar{T}$ [K] averaged over latitudes north of 80°N at 10 hPa. The SSW events are numbered as shown in the first column of Table 1. Figure 5b shows the resultant predictability limits for 126 ensemble forecasts performed during the five winter seasons. In the undisturbed phase (white squares) predictability limits are significantly long, owing to small values of the RMSE themselves. In these cases, the predictability limits are long, but these forecasts have no practical skill, because the RMSE tends to be saturated before reaching the threshold value, i.e., 232 m (see Fig. 2b).

In the disturbed phase (black squares) predictability limits range over 3–19 days according to the case. The predictability limit averaged over 98 ensemble forecasts in the disturbed phase is about 10.4 days. In addition, it is interesting to note that the predictability limit for the SSW in late January 2003 (No. 5 in Table 1) was much shorter than the average. The prominent WN-2 planetary waves contributed to this SSW as mentioned above. When stratospheric circulations change suddenly and greatly, precise prediction is difficult and predictability limits tend to be short.

Furthermore, the alternative predictability limit is evaluated on the basis of the AC defined by Eq. (3) using the low-pass filtered field for z_{ci}, in order to examine the similarity of synoptic patterns. An AC score of 1.0 means perfect skill and it decreases with forecast time. As mentioned in Section 3.2, the time when the AC first reaches the threshold is defined as a predictability limit. The threshold value in the stratosphere is here set to 0.6, which is commonly used in the troposphere. Figure 5c shows the resultant predictability limits estimated by using the AC. In the disturbed phase, the predictability limit is almost the same as that of the RMSE. The mean predictability limit of 98 ensemble forecasts in the disturbed phase is about 9.4 days. On the other hand, in the undisturbed phase, the predictability limits are almost the same as those in the disturbed phase. This is a totally different feature from that of the predictability limit based on the RMSE as shown in Fig. 5b.

Finally, plausible causes of the variable predictability limit based on the RMSE are examined in detail. Here, by using the method described in Section 3.3, we discuss each contribution of the forecast error associated with the zonal-mean field, the wave amplitude and the wave phase to the mean square error at the time when the RMSE attains the predictability limit in the disturbed phase.

Figure 6 denotes contribution ratios of forecast errors in the zonal-mean field (yellow), the wave amplitude (red), and the wave phase (black) at the time when each forecast reaches the predictability limit based on the RMSE. Fig. 6a shows results of forecasts starting from Wednesday, while Fig. 6b represents those starting from Thursday. Ratios from Wednesday occasionally differ from those from Thursday, because of the difference of initial conditions for the prediction between Wednesday and Thursday.

Though causes of poor prediction depend on the case, the enlarged RMSE is caused by unskillful prediction of not only wave amplitude and wave phase but also of zonal-mean components. On average, the contribution ratios of the zonal-mean field, the wave amplitude, and the wave phase to forecast errors during the disturbed phase are 0.348,

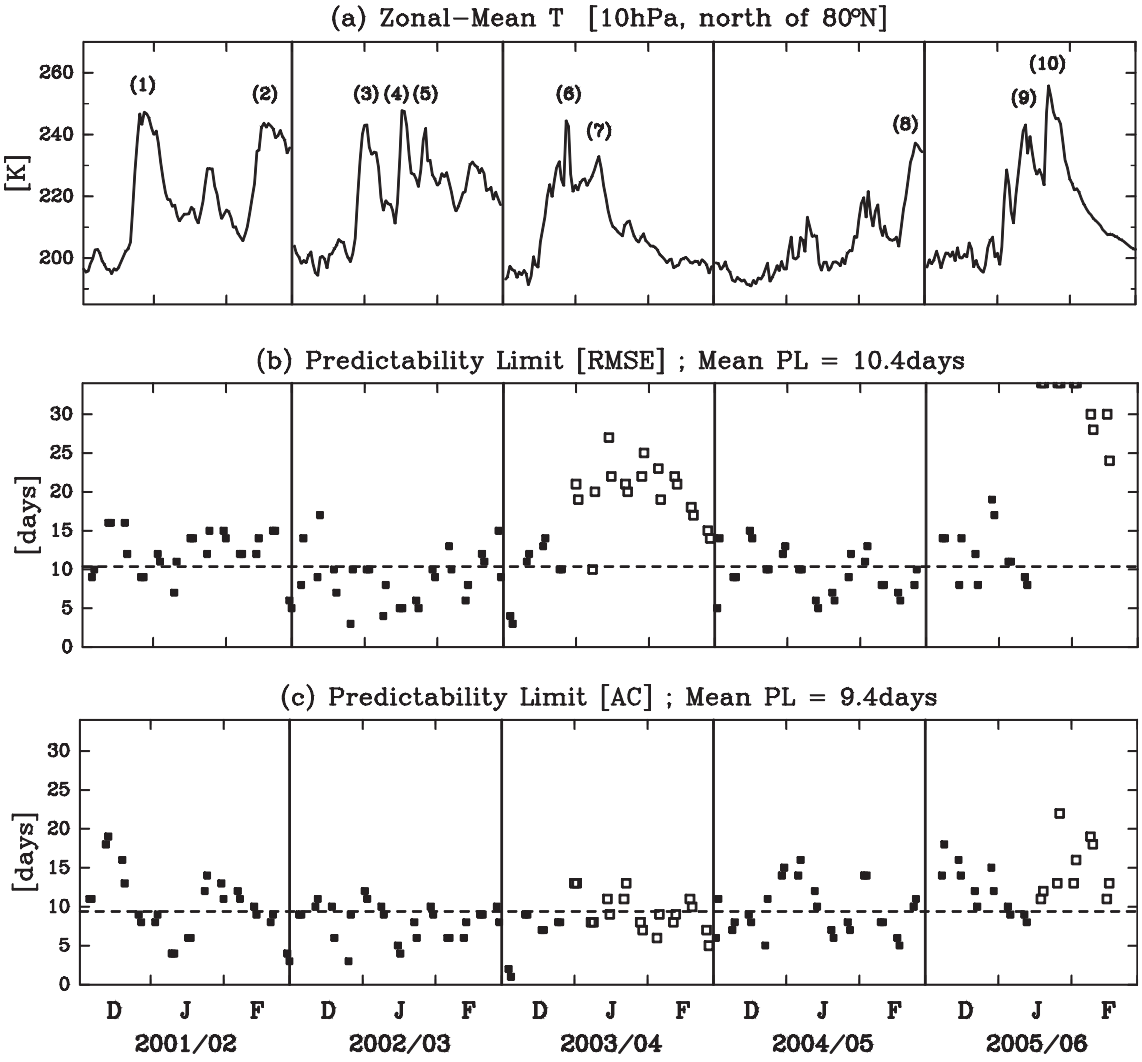

Fig. 5. (a) Time variation of observed $\overline{T}$ [K] averaged over latitudes north of 80°N at 10 hPa. SSW events are numbered as shown in Table 1. (b) and (c) show the predictability based on the RMSE and AC for 126 ensemble forecasts performed during the five winters, respectively. Black (white) squares show the predictability limit during the disturbed (undisturbed) phase. The broken horizontal line indicates the averaged predictability over the disturbed phase. The abscissa in (b) and (c) denotes the initial time of each forecast.

0.296, and 0.355, respectively. Hence, the wave phase relatively dominates the RMSE, but the zonal mean field also plays a significant role. The ratio of the zonal-mean field tends to be large when the basic flow dramatically changes. For instance, the polar zonal-mean heights during SSW events are higher than those during no-SSW events. Contrarily, those during the strong vortex periods with relatively weak planetary wave activity, such as February 2005, are lower than the climatology. Such a rise (fall) of polar heights tend to be predicted lower (higher) than the observed one. These unskillful predictions of zonal-mean components greatly contribute to the enlargement of the RMSE (shortening of the predictability limit in Fig. 5b).

Moreover, the RMSE caused by poor prediction of waves and zonal-mean fields is hardly amplified simultaneously (not shown). The difference of these time evolutions between waves and zonal-mean fields is explained by the fact that intensified planetary waves firstly propagate from the troposphere to bring about breakup of the polar vortex in the upper strato-

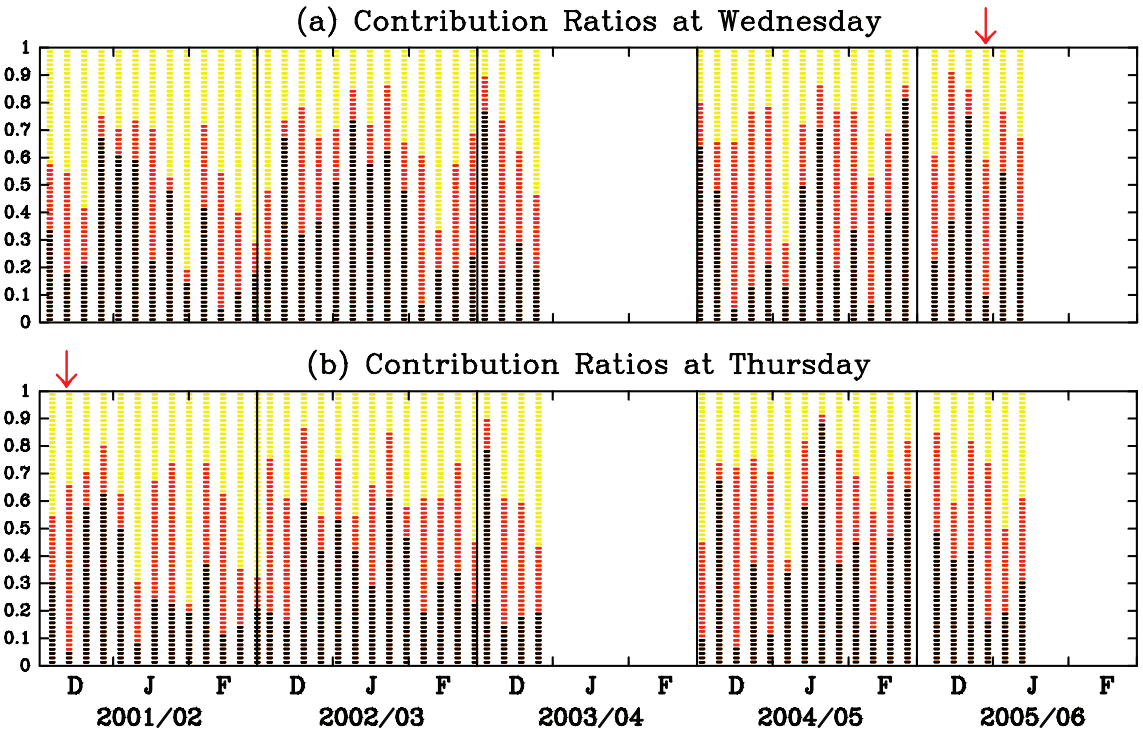

Fig. 6. Contribution ratios of forecast errors in the zonal mean field (yellow), the wave amplitude (red) and the wave phase (black) at the time when each forecast reaches the predictability limit based on the RMSE. Forecasts start from (a) Wednesday and (b) Thursday in the disturbed phase. The abscissa denotes the initial time of each forecast. Predictions for Nos. 1 and 9 in Table 1 are marked by the red arrows.

sphere, which is followed by changes of the zonal-mean height in the polar region of lower levels (e.g., Matsuno and Nakamura 1979).

5.2 *Predictability of SSW occurrence*

In this section, we examine the predictability of the occurrence of SSWs. Here, we investigate the predicted $\bar{T}$ at 80°N and 10 hPa for the forecasts initialized about two weeks before the warming peaks of SSWs shown in Table 1 using all ensemble members.

Figure 7 shows the time evolution of $\bar{T}$ of these forecasts. A thick red line denotes the observation and the warming peak is located at day 0. A thin red line and a thin blue line denote the ensemble mean and the unperturbed forecast, respectively, while thin black lines denote all 12 perturbed members. From these panels, it is found that most forecasts cannot successfully predict the warming peaks in viewpoints of either timing or magnitude. These forecasts have large variability among ensemble members at the warming peak. However, all forecasts initialized one week after could successfully predict warming peaks (not shown). Hence, it can be said that the warming peaks are roughly predictable from 1-2 weeks in advance. By contrast, the ensemble forecast in December 2001 skillfully predicts the warming peak with fairly suppressed spread (No. 1 in Fig. 7). Also the forecast at the beginning of January 2006 can skillfully predict the warming peak, though the variability is somewhat large (No. 9 in Fig. 7). Hence, it can be concluded that in these two cases the warming peaks are predictable at least from two weeks in advance.

Next, we consider the relation between the predicted $\bar{T}$ change and the predictability limits of stratospheric circulations. The RMSE is greatly influenced by the forecast errors due to zonal-mean fields as shown in Section 5.1, while the AC is little affected by zonal-mean fields because it indicates the measure for the predicted pattern. Therefore, we consider here the predictability limits based on the RMSE.

The fourth column in Table 1 denotes the predictability limit based on the RMSE of forecasts initialized about two weeks before each warming peak.

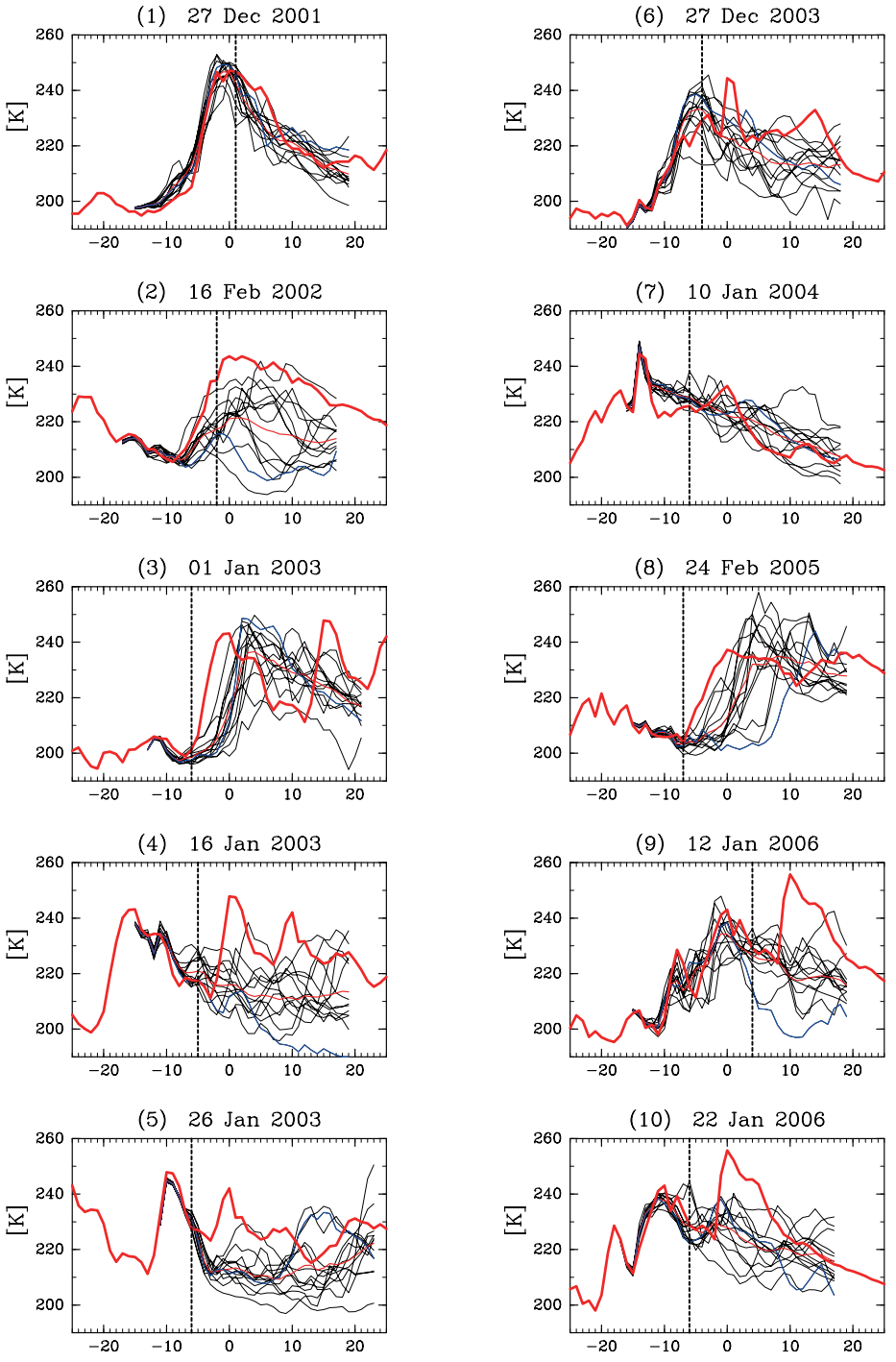

Fig. 7. Predicted $\overline{T}$ [K] averaged over latitudes north of 80°N at 10 hPa for each SSW event. Each forecast is initialized about two weeks before the warming peaks shown in Table 1. The date of the warming peak is shown in the title of each panel. A thick red line denotes the observation and the warming peak is located at day 0. A thin red line and a thin blue line denote the ensemble mean and the unperturbed forecast, respectively, while thin black lines denote all 12 perturbed members. The vertical broken line represents each predictability limit based on the RMSE shown in the fourth column of Table 1.

We can see events of Nos. 1, 2, and 9 in Table 1 have predictability limits of longer than two weeks (the fourth column in Table 1). Moreover, the predictability limits are compared with "lead time" which is defined as the time length from the initial time of the forecast to each warming peak (the third column in Table 1). If the predictability limit is longer (shorter) than the lead time, the warming peak might be successfully (unskillfully) predicted. From this viewpoint, it is considered that the only cases of Nos. 1 and 9 in Table 1 were able to predict the warming peak. In fact, this expectation is consistent with results of Fig. 7; the predictability limits shown by vertical broken lines in Fig. 7 are mostly located before the warming peaks at day 0 except for Nos. 1 and 9. Additionally, after the prediction time exceeds the predictability limit, the spread among ensemble members becomes large and the ensemble-mean forecasts start to be unskilled.

Furthermore, an interesting feature for the predicted $\bar{T}$ can be seen in the cooling period after SSW events. Figure 8 indicates time variations of the 10-hPa $\bar{T}$ averaged over latitudes north of 80°N for forecasts starting just after each warming peak. The date of the warming peak is shown in the title line of each panel. As in Fig. 7, the thick red lines denote the observation while the thin red, blue and black lines are the ensemble mean, unperturbed and perturbed members, respectively. Note that forecasts for Nos. 6, 7, 9, and 10 of Fig. 8 started from the undisturbed phase while the others started from the disturbed phase (all forecasts in Fig. 7 started from the disturbed phase). In particular, the forecast periods of Nos. 7 and 10 in Fig. 8 corresponds to the cooling phase after the peak of the SSW event. It is found that the ensemble spread during a forecast period of about 10 days, which roughly corresponds to the predictability limit obtained from Fig. 5, for these predictions starting from the undisturbed phase is smaller than that of forecast starting from the disturbed phase.

The reduced spread along with the relatively longer predictability limit, based on the RMSE evolution in Fig. 5b, reveals that the cooling process during the attenuation period of the SSW is more skillfully predicted in comparison with the disturbed phase. This is in line with the observation obtained in Noguchi et al. (2014) by examining month-to-month predictability variations of the North Pole temperature in the stratosphere.

It is interesting to examine the change in the predictability during the transition from the disturbed phase to the undisturbed one across the warming peak (from Nos. 6, 7, 9, and 10 in Fig. 7 to those in Fig. 8) in comparison with the change across the warming peak without accompanying the phase transition (Nos. 1, 2, 3, 4, 5, and 8). From this comparison, we notice that the ensemble spread during a forecast period of about 10 days does not shrink remarkably for the latter cases even for the attenuation period of the SSW, compared with the former events where the spread shrinks. This suggests that physical processes relevant to the attenuation of the SSW are not common to all SSW events.

In the former events, the radiative process would be the primary factor for the cooling process during the attenuation period. On the other hand, for the latter events of which attenuation period is characterized by the disturbed phase, any other dynamical processes would play an important role. One of the most plausible factors would be the change of the propagation direction of stratospheric planetary waves from the upward to equatorward in association with the quick recovery of the polar night jet after the warming peak. In fact, such evolution in the propagating property of planetary waves was observed just after the warming peak of the SSW in February 2007 as reported by Kodera et al. (2008). We need further detailed analysis on the change of predictability and the related dynamics during the transition from the disturbed to undisturbed phase.

6. Discussion and conclusions

In the present study, the stratospheric predictability in the boreal winter has been examined using the archive of 1-month ensemble forecast datasets provided by JMA. It has been investigated on the basis of both the RMSE and the AC of the 10-hPa geopotential height during 2001–2006.

Features of the atmospheric circulation are quite different between the troposphere and the stratosphere in winter. Such differences are caused by different predominant waves in each level: In the troposphere, baroclinic waves are almost always predominant throughout every winter season. On the other hand, in the stratosphere, amplified planetary waves intermittently propagate from the troposphere. These features induce different characteristics of the predictability between the troposphere and the stratosphere, when these are investigated by using the RMSE which represents forecast errors focusing on large-scale atmospheric motions. A prominent difference is seen in the variability of the RMSE (Fig. 2): The time evolution of the RMSE in the troposphere

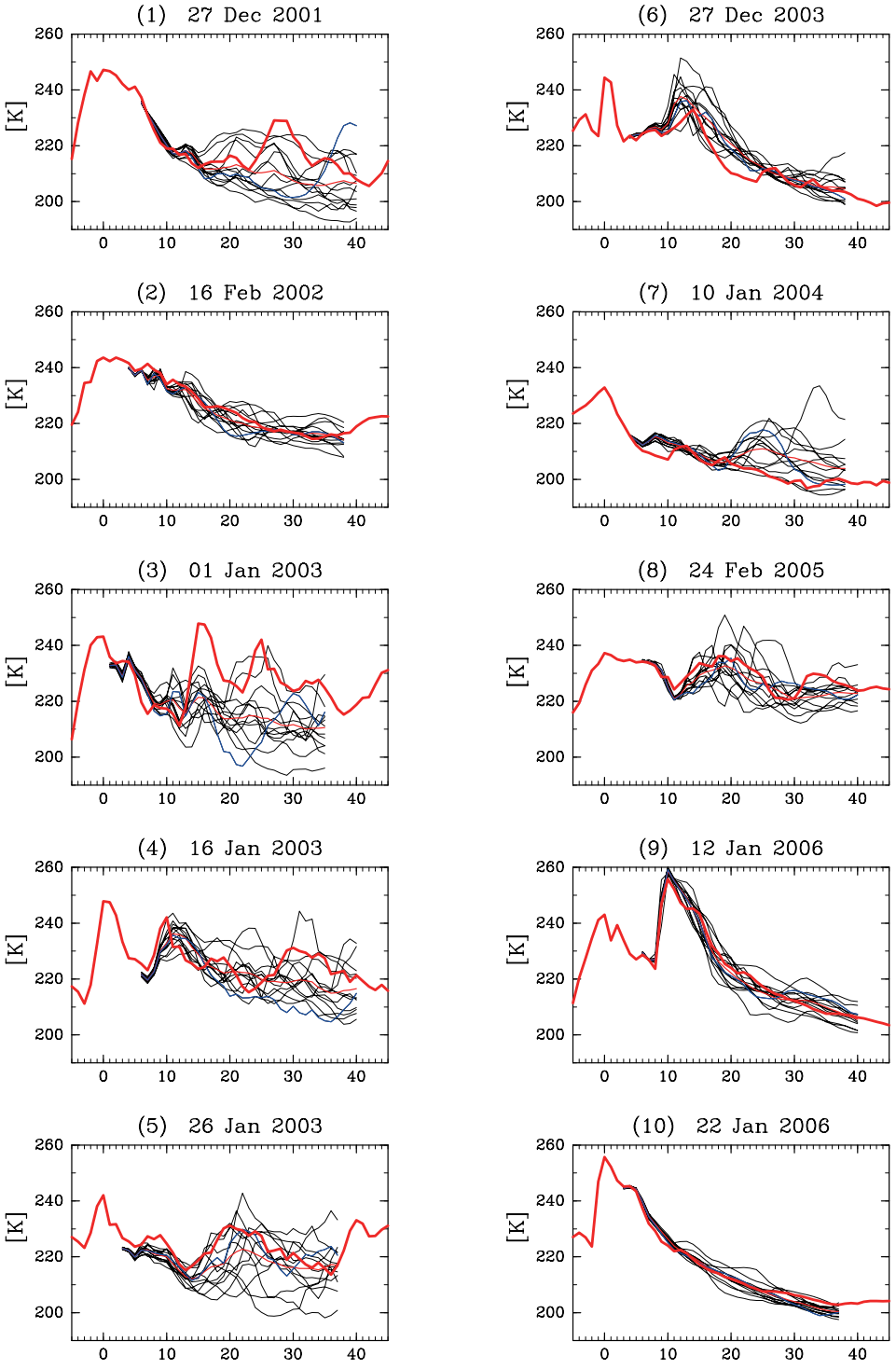

Fig. 8. Time variations of the 10-hPa $\bar{T}$ [K] averaged over latitudes north of 80°N for forecasts starting just after each warming peak corresponding to day 0, of which the date is shown in the title of each panel. A thick red line represents the observation. A thin red line and a thin blue line denote the ensemble mean and the unperturbed forecast, respectively, while thin black lines denote all 12 perturbed members.

is similar among forecasts, while that in the stratosphere greatly depends on the case. It is considered that the large variation in the stratosphere is caused by the intermittent propagation of planetary waves.

Another interesting result is that the predictable period in the stratosphere is generally longer than that in the troposphere. It is probably reflected by the fact that the predictability limit of planetary waves is longer than that of synoptic waves.

In the undisturbed phase, especially after major warmings, planetary waves do not propagate up to the stratosphere (see Fig. 1) even if planetary waves are amplified in the troposphere, because they exponentially decay in easterlies (Charney and Drazin 1961). Therefore, the RMSE of the stratospheric circulation itself becomes small and tends to be saturated before reaching the threshold value for the predictability limit, making the predictability limits based on the RMSE quite long (Fig. 5b). However, those based on the AC are almost the same as those in the disturbed phase (Fig. 5c). It implies that a synoptic pattern for the prediction period exceeding the predictability limit based on the AC is not skillfully predicted although the RMSE does not reach the threshold value.

Focusing on the time evolution of the predicted $\overline{T}$ in the undisturbed phase, we found that the cooling process after SSW events seems to be well predicted during the whole forecast (Fig. 8). In this case, the pattern is less predictable, though the RMSE is small and the predictability limit based on the RMSE is quite long.

In the disturbed phase, when planetary waves propagate into the stratosphere, the mean predictability limit based on the RMSE is 10.4 days, while that based on the AC is 9.4 days, i.e., shorter than that based on the RMSE by 1 day. A similar result was also reported for the tropospheric predictability limit (Hollingsworth et al. 1978). Therefore, it is considered that the relationship of the predictability limits between RMSE and AC analyses is the same for the stratosphere and the troposphere.

When we focus on the occurrence of SSW events, it is found that poor predictions of not only waves but also zonal-mean field greatly contribute to the growth of forecast errors (Fig. 6); this was not pointed out by previous studies (e.g., MH04; Stan and Straus 2009).

In addition, when the prediction of warming peaks is focused, there are cases whose predictability limit based on the RMSE exceeds two weeks, such as the cases of December 2001 and the beginning of January 2006 (see Nos. 1 and 9 in Table 1). In these forecasts, forecast errors due to the phase difference tends to be very small (see red arrows of Fig. 6). For further studies, we have to elucidate the mechanism producing such enhanced predictability for the phase of WN-1 planetary waves in the framework of stratosphere-troposphere dynamical coupling.

There is a case whose predictability limits based on the RMSE are less than a week, such as the event of late January 2003 (see No. 5 in Table 1). In this case, WN-2 waves as well as WN-1 ones are prominent. Hirooka et al. (2007) also discussed that the prediction of the WN-2 and WN-3 evolutions was difficult for the SSW event of January 2004 (see No. 7 in Table 1). On the other hand, Marshall and Scaife (2010) examined the predictable period of two vortex-splitting-type SSW events (December 1987 and February 1999) and two vortex-displacement-type SSW events by conducting hindcast experiments initialized at 1-day interval with a Hadley Center atmospheric general circulation model (HadGAM1). The obtained result (see Table 1 of Marshall and Scaife 2010), however, does not show any significant differences in the predictable period for the two SSW types. Hence, we have to conduct more detailed ensemble hindcast experiments for a larger sample of SSW events to elucidate what features of SSW determine the predictable period in future studies.

Acknowledgments

This work was partly supported by Grants-in-Aid for Scientific Research (24340113, 26287115, and 24224011) from Japan Society of Promotion of Science, and also by the general collaborative research funded from the Disaster Prevention Research Institute, Kyoto University. TI and SN were supported by Research Fellowships of the Japan Society for the Promotion of Science for Young Scientists. We would like to thank all members in the Climate Prediction Division in JMA for providing the datasets. We extend our thanks to Ryo Mizuta at the Meteorological Research Institute for his kind offer of the information on the JMA forecast model. Comments provided by two anonymous reviewers and the editor, to improve the manuscript, are gratefully acknowledged. The GFD-DENNOU Library was used for drawing the figures.

References

Baldwin, M. P., and T. J. Dunkerton, 2001: Stratospheric

harbingers of anomalous weather regimes. *Science*, **294**, 581–584.

Boville, B. A., 1984: The influence of the polar night jet on the tropospheric circulation in a GCM. *J. Atmos. Sci.*, **41**, 1132–1142.

Briegleb, B. P., 1992: Delta-eddington approximation for solar radiation in the NCAR community climate model. *J. Geophys. Res.*, **97**, 7603–7612.

Charlton, A. J., and L. M. Polvani, 2007: A new look at stratospheric sudden warmings. Part I: Climatology and modeling benchmarks. *J. Climate*, **20**, 449–469.

Charney, J. G., and P. G. Drazin, 1961: Propagation of planetary-scale disturbances from the lower into the upper atmosphere. *J. Geophys. Res.*, **66**, 83–109.

Coakley, J. A., R. D. Cess, and F. B. Yurevich, 1983: The effect of tropospheric aerosols on the earth's radiation budget: A parameterization for climate models. *J. Atmos. Sci.*, **40**, 116–138.

Hirooka, T., T. Ichimaru, and H. Mukougawa, 2007: Predictability of stratospheric sudden warmings as inferred from ensemble forecast data: Intercomparison of 2001/02 and 2003/04 winters. *J. Meteor. Soc. Japan*, **85**, 919–925.

Hollingsworth, A., K. Arpe, M. Tiedtke, M. Capaldo, H. Savijarvi, O. Akesson, and J. A. Woods, 1978: *Comparison of medium range forecasts made with two parameterization schemes*. ECMWF Tech. Rep., **13**, 214 pp.

Inatsu, M., N. Nakano, S. Kusuoka, and H. Mukougawa, 2015: Predictability of wintertime stratospheric circulation examined using a nonstationary fluctuation-dissipation relation. *J. Atmos. Sci.*, **72**, 774–786.

Iwasaki, T., S. Yamada, and K. Tada, 1989: A parameterization scheme of orographic gravity wave drag with two different vertical partitionings. Part I: Impacts on medium-range forecasts. *J. Meteor. Soc. Japan*, **67**, 11–27.

Japan Meteorological Agency, 2002: *Outline of the operational numerical weather prediction at the Japan Meteorological Agency.* Appendix to WMO Numerical Weather Prediction Progress Report, Japan Meteorological Agency, 157 pp.

Kalnay, E., 2003: *Atmospheric Modeling, Data Assimilation and Predictability.* Cambridge University Press, 341 pp.

Kidston, J., A. A. Scaife, S. C. Hardiman, D. M. Mitchell, N. Butchart, M. P. Baldwin, and L. J. Gray, 2015: Stratospheric influence on tropospheric jet streams, storm tracks and surface weather. *Nat. Geosci*., **8**, 433–440.

Kimoto, M., H. Mukougawa, and S. Yoden, 1992: Medium-range forecast skill variation and blocking transition: A case study. *Mon. Wea. Rev.*, **120**, 1616–1627.

Kodera, K., K. Yamazaki, M. Chiba, and K. Shibata, 1990: Downward propagation of upper stratospheric mean zonal wind perturbation to the troposphere. *Geophys. Res. Lett.*, **17**, 1263–1266.

Kodera, K., H. Mukougawa, and S. Itoh, 2008: Tropospheric impact of reflected planetary waves from the stratosphere. *Geophys. Res. Lett.*, **35**, L16806, doi:10.1029/2008GL034575.

Kuroda, Y., 2008: Role of the stratosphere on the predictability of medium-range weather forecast: A case study of winter 2003-2004. *Geophys. Res. Lett.*, **35**, L19701, doi:10.1029/2008GL034902.

Labitzke, K. G., and H. van Loon, 1999: *The Stratosphere: Phenomena, History, and Relevance.* Springer-Verlag, 179 pp.

Lorenz, E. K., 1963: Deterministic nonperiodic flow. *J. Atmos. Sci.*, **20**, 130–141.

Marshall, A. G., and A. A. Scaife, 2010: Improved predictability of stratospheric sudden warming events in an atmospheric general circulation model with enhanced stratospheric resolution. *J. Geophys. Res.*, **115**, D16114, doi:10.1029/2009JD012643.

Matsuno, T., 1971: A dynamical model of the stratospheric sudden warming. *J. Atmos. Sci.*, **28**, 1479-1494.

Matsuno, T., and K. Nakamura, 1979: The Eulerian- and Lagrangian- mean meridional circulations in the stratosphere at the time of sudden warming. *J. Atmos. Sci.*, **36**, 640–654.

Mechoso, C. R., K. Yamazaki, A. Kitoh, and A. Arakawa, 1985: Numerical forecasts of stratospheric warming events during the winter of 1979. *Mon. Wea. Rev.*, **113**, 1015–1029.

Mukougawa, H., and T. Hirooka, 2004: Predictability of stratospheric sudden warming: A case study for 1998/99 winter. *Mon. Wea. Rev.*, **132**, 1764–1776.

Mukougawa, H., H. Sakai, and T. Hirooka, 2005: High sensitivity to the initial condition for the prediction of stratospheric sudden warming. *Geophys. Res. Lett.*, **32**, L17806, doi:10.1029/2005GL022909.

Noguchi, S., H. Mukougawa, T. Hirooka, M. Taguchi, and S. Yoden, 2014: Month-to-month predictability variations of the winter-time stratospheric polar vortex in an operational one-month ensemble prediction system. *J. Meteor. Soc. Japan*, **92**, 543–558.

Reichler, T., P. J. Kushner, and L. M. Polvani, 2005: The coupled stratosphere-troposphere response to impulsive forcing from the troposphere. *J. Atmos. Sci.*, **62**, 3337–3352.

Scherhag, R., 1952: Die explosionsartige stratosphärenerwärmungen des spätwinters 1951/52. *Ber. Deut. Wetterdienst*, **38**, 51–63.

Stan, C., and M. Straus, 2009: Stratospheric predictability and sudden stratospheric warming events. *J. Geophys. Res.*, **114**, L12103, doi:10.1029/2008JD011277.

Swinbank, R., and A. O'Neill, 1994: A stratosphere-troposphere data assimilation system. *Mon. Wea. Rev.*, **122**, 686–702.

Toth, Z., and E. Kalnay, 1993: Ensemble forecasting at

NMC: The generation of perturbations. *Bull. Amer. Meteor. Soc.*, **74**, 2317–2330.

Tripathi, O. P., M. Baldwin, A. Charlton-Perez, M. Charron, S. D. Eckermann, E. Gerber, R. G. Harrison, D. R. Jackson, B.-M. Kim, Y. Kuroda, A. Lang, S. Mahmood, R. Mizuta, G. Roff, M. Sigmond, and S.-W. Son, 2015: The predictability of the extratropical stratosphere on monthly time-scales and its impact on the skill of tropospheric forecasts. *Quart. J. Roy. Meteor. Soc.*, **141**, 987–1003.